Journal of Physics: Conference Series **3190** (2026) 012013 doi:10.1088/1742-6596/3190/1/012013

Exploring Stability Domains in Compressible Ogden's Hyperelastic Model

Attila Kossa

Department of Applied Mechanics,
Faculty of Mechanical Engineering,
Budapest University of Technology and Economics, Budapest, Hungary

E-mail: kossa@mm.bme.hu

Abstract. Rubber-like materials significantly affect the vibrational behavior and damping behavior of structures. Precise numerical computations in vibroacoustic engineering call for precise modeling of rubber-like materials. The most frequently utilized constitutive mechanical models for such materials are the hyperelastic models, of which the Ogden model is extremely popular since it can simulate well nonlinear stress-strain behavior using a very low number of material parameters. In practical applications, the accounting of volumetric deformation, however small, is crucial to achieve proper simulation. The present study demonstrates that for the compressible Ogden model, the loss of transverse strain stability may occur even under uniaxial loading conditions, potentially leading to numerical difficulties in simulations. The research aims at determining the regions of transverse strain stability for common loading conditions and examining the influence of Poisson's ratio on these stability regions. Through the application of analytical as well as numerical methods, we obtain such stability boundaries. Such knowledge of stability limits is significant to ensure that efficient numerical solutions can be obtained in engineering applications. These findings can directly be utilized in improving the accuracy of NVH simulations where rubber components (such as bushings, mounts, or seals) are utilized in vibration isolation and structural noise absorption in vehicles. Our findings provide valuable guidance on enhancing the accuracy of acoustic and vibrational design models, bridging theory with practical engineering needs.

1 Introduction

For modeling the nonlinear elastic behavior of rubber-like materials under large deformations, hyperelastic material models are typically employed [3, 6]. Since rubber materials are approximately incompressible, in some applications this assumption can be utilized, allowing the use of so-called incompressible hyperelastic models. Numerous such models can be found in the literature [2, 7].

In reality, however, a certain degree of volumetric deformation is always present. Therefore, for more accurate finite element simulations, it is essential to use compressible hyperelastic models for rubber materials. This becomes especially important in loading scenarios where the material's deformation is highly constrained, such as in rubber mountings or seals. In cases involving small volumetric deformations (nearly incompressible, slightly compressible), the volumetric part of the strain energy density function often takes a relatively simple form.

Nevertheless, for the compressible hyperelastic models commonly used in the literature, it is generally true that even in basic loading cases, a closed-form solution for the stress response cannot be derived. As a result, analytical investigations of the models' behavior become challenging. It is worth noting, in contrast, that for incompressible hyperelastic models, closed-form stress solutions can often be obtained, enabling analytical studies such as determining the Drucker-type stability limits [4].

The simplest hyperelastic model is the neo-Hookean model, which, in the incompressible case, contains only a single material parameter. A detailed analysis of its compressible version was recently published in a journal article [5], where the authors not only derived the full stress–stretch relations but also performed a systematic stability analysis, showing that, depending on the parameters, multiple solutions may emerge for the transverse stretch even under simple loading. A similar type of stability loss, together with a complete analytical discussion of the associated instability mechanism, was later also demonstrated for the Mooney–Rivlin model in another study [1].

The Ogden hyperelastic model is perhaps one of the most widely used models [6]. This model family includes both the neo-Hookean and the Mooney–Rivlin models as special cases. Even the first-order Ogden model can approximate highly nonlinear stress-strain behavior with relatively good accuracy, which makes it a popular constitutive model in industrial applications.

The present manuscript investigates stability loss in transverse deformation for the first-order Ogden hyperelastic model formulated for the compressible case. For three basic loading scenarios, we determine the critical stretch and model parameter values where the material model exhibits loss of transverse strain stability. With the new results, one can avoid parameter combinations that would otherwise lead to undesirable instabilities at the material model level. Consequently, more reliable numerical simulations can be performed.

Accurate modeling of rubber materials is of paramount importance in NVH engineering, where such materials are heavily employed to isolate vibrations and reduce noise transmission in vehicles. The stability of the hyperelastic model employed directly influences the reliability of time-domain and frequency-domain simulations. Understanding and avoiding parameter sets that cause instability is hence crucial for sound vehicle dynamics modeling and vibration-isolating component design.

2 Compressible, isotropic, Ogden hyperelastic model

Several versions of the Ogden hyperelastic model formulated for the compressible case can be found in the literature. The most commonly used variant is the one implemented as a built-in material model in the Abaqus finite element software. In this model, the strain energy density function is given as follows:

$$U = \sum_{k=1}^{N} \frac{2\mu_k}{\alpha_k^2} \left(\bar{\lambda}_1^{\alpha_k} + \bar{\lambda}_2^{\alpha_k} + \bar{\lambda}_3^{\alpha_k} - 3\right) + \sum_{k=1}^{N} \frac{1}{D_k} \left(J-1\right)^{2k}, \tag{1}$$

where N is a positive integer denoting the order of the model, and the parameters α_k, μ_k, and D_k are the material constants. Thus, an N-th order model contains a total of $3N$ parameters.

Journal of Physics: Conference Series **3190** (2026) 012013 doi:10.1088/1742-6596/3190/1/012013

In the expression for U, the quantities $\bar{\lambda}_i$ denote the modified (or distortional or deviatoric) principal stretches, which are derived from the principal stretches using the volume ratio J, as follows:

$$\bar{\lambda}_i = J^{-1/3}\lambda_i = (\lambda_1\lambda_2\lambda_3)^{-1/3}\,\lambda_i \tag{2}$$

with $i = 1, 2, 3$. Once U is known, the Cauchy stress tensor can be computed in the following form:

$$\boldsymbol{\sigma} = \frac{1}{J}\sum_{i=1}^{3}\lambda_i\frac{\partial U}{\partial\lambda_i}\boldsymbol{n}_i\otimes\boldsymbol{n}_i = \sum_{i=1}^{3}\sigma_i\boldsymbol{n}_i\otimes\boldsymbol{n}_i, \tag{3}$$

where $\boldsymbol{n}_i$ denotes the Eulerian principal directions (unit vectors), and σ_i are the corresponding principal stress components. If we consider the first-order version of the model ($N = 1$), the strain energy density function simplifies to:

$$U = \frac{2\mu}{\alpha^2}\left(\bar{\lambda}_1^{\alpha} + \bar{\lambda}_2^{\alpha} + \bar{\lambda}_3^{\alpha} - 3\right) + \frac{1}{D}\left(J-1\right)^2. \tag{4}$$

In the present study, all stability analyses are carried out exclusively for this first-order case. In order to simplify the forthcoming expressions, we introduce the notations: $\mu = \mu_1$, $\alpha = \alpha_1$, $D = D_1$. By substituting the definitions of the modified principal stretches and the relation between the volume ratio and the principal stretches, we finally obtain the following form for U:

$$U = \frac{2\mu}{\alpha^2}\left(\frac{\lambda_1^{2\alpha/3}}{(\lambda_2\lambda_3)^{\alpha/3}} + \frac{\lambda_2^{2\alpha/3}}{(\lambda_1\lambda_3)^{\alpha/3}} + \frac{\lambda_3^{2\alpha/3}}{(\lambda_1\lambda_2)^{\alpha/3}} - 3\right) + \frac{1}{D}\left(\lambda_1\lambda_2\lambda_3 - 1\right)^2. \tag{5}$$

From the function U, the nominal stress (also known as engineering stress or first Piola–Kirchhoff stress) components can also be easily computed using the following formulas:

$$P_1 = \frac{\partial U}{\partial\lambda_1}, \qquad P_2 = \frac{\partial U}{\partial\lambda_2}, \qquad P_3 = \frac{\partial U}{\partial\lambda_3}. \tag{6}$$

If $\alpha = 2$, the first-order Ogden model simplifies to the neo-Hookean model, whose detailed analysis can be found in the literature [5]. It is important to note that the case $\alpha = 0$ is not allowed, as the model becomes singular; nevertheless, α can, in general, take any real value. It is also worth mentioning that while the Mooney–Rivlin model cannot be recovered from the first-order ($N = 1$) Ogden formulation, it can be obtained as a special case of the Ogden model when $N = 2$ by an appropriate choice of the material parameters.

3 Homogeneous loading modes

We examine three types of homogeneous loading: uniaxial loading, equibiaxial loading, and planar loading. These loading scenarios are illustrated in Fig. 1. They represent the standard cases typically used for evaluating hyperelastic material models. All three loading types are characterized by a plane stress condition ($\sigma_3 = 0$). As a result, the Cauchy stress tensor can be expressed in matrix form, in the principal directions coordinate system, as follows:

$$[\boldsymbol{\sigma}] = \begin{bmatrix} \sigma_1 & 0 & 0 \\ 0 & \sigma_2 & 0 \\ 0 & 0 & 0 \end{bmatrix}. \tag{7}$$

In the uniaxial case, we have $\sigma_1 = \sigma$ and $\sigma_2 = 0$; in the equibiaxial case, $\sigma_1 = \sigma_2 = \sigma$; and in the planar case, $\sigma_1 = \sigma$ and $\sigma_2 \neq 0$. The corresponding deformation gradients ($\boldsymbol{F}$) and principal stretches for each loading case are summarized below. For notational simplicity, we denote the transverse stretch in the third direction as λ_T, while λ refers to the stretch in the loading direction.

Uniaxial loading:

$$[\boldsymbol{F}] = \begin{bmatrix} \lambda & 0 & 0 \\ 0 & \lambda_T & 0 \\ 0 & 0 & \lambda_T \end{bmatrix}, \ \lambda_1 = \lambda, \ \lambda_2 = \lambda_3 = \lambda_T. \tag{8}$$

Equibiaixial loading:

$$[\boldsymbol{F}] = \begin{bmatrix} \lambda & 0 & 0 \\ 0 & \lambda & 0 \\ 0 & 0 & \lambda_T \end{bmatrix}, \ \lambda_1 = \lambda_2 = \lambda, \ \lambda_3 = \lambda_T. \tag{9}$$

Planar loading:

$$[\boldsymbol{F}] = \begin{bmatrix} \lambda & 0 & 0 \\ 0 & 1 & 0 \\ 0 & 0 & \lambda_T \end{bmatrix}, \ \lambda_1 = \lambda, \ \lambda_2 = 1, \ \lambda_3 = \lambda_T. \tag{10}$$

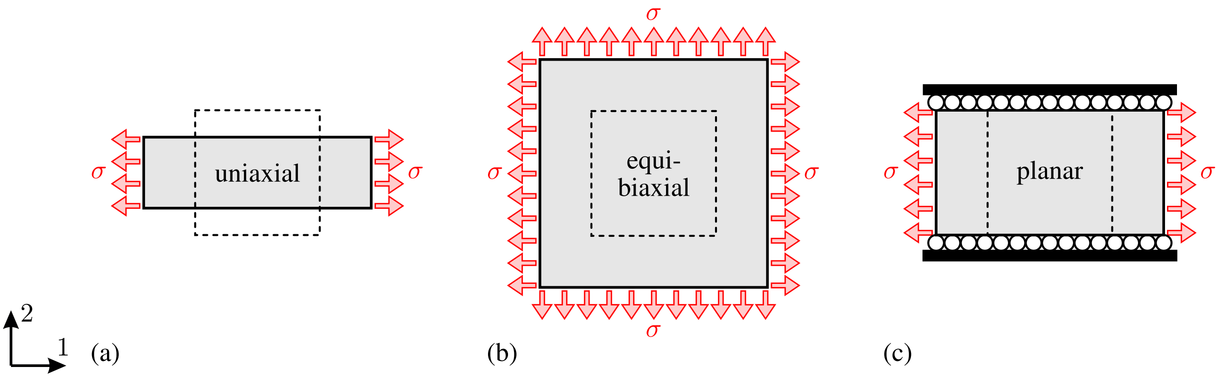

Figure 1: Schematic representation of the investigated loading cases. (a) Uniaxial loading. (b) Equibiaxial loading. (c) Planar loading.

4 Ground-state Poisson's ratio

From the material parameters of the hyperelastic model, expressions for the ground-state moduli can be derived. In this section, our goal is to determine the expression of the Poisson's ratio in terms of the model parameters. From a practical perspective, it is important to understand which parameters must be selected in the hyperelastic model in order to represent a material characterized by a given Poisson's ratio. The introduction and use of the ground-state moduli are well established in the hyperelasticity literature

To determine the ground-state Poisson's ratio, we linearize the model around the undeformed (initial) configuration under uniaxial loading. For uniaxial loading, the principal nominal stress components are given by the following expressions (based on Eq. 6):

$$P_1 = \frac{4\mu}{3\alpha\lambda}\left(\frac{\lambda^{2\alpha/3}}{\lambda_T^{2\alpha/3}} - \frac{\lambda_T^{2\alpha/3}}{(\lambda\lambda_T)^{\alpha/3}}\right) + \frac{2\lambda_T^2}{D}\left(\lambda\lambda_T^2 - 1\right), \tag{11}$$

$$P_2 = P_3 = \frac{2\mu}{3\alpha\lambda_T}\left(\frac{\lambda_T^{2\alpha/3}}{(\lambda\lambda_T)^{\alpha/3}} - \frac{\lambda^{2\alpha/3}}{\lambda_T^{2\alpha/3}}\right) + \frac{2\lambda\lambda_T}{D}\left(\lambda\lambda_T^2 - 1\right). \tag{12}$$

Journal of Physics: Conference Series **3190** (2026) 012013 doi:10.1088/1742-6596/3190/1/012013

It is important to note that due to the boundary conditions, we have $P_2 = P_3 = 0$. To distinguish the linearized case, we denote the resulting stress components with a tilde. The linearized stress expressions are then calculated as:

$$\tilde{\sigma}_1 = \left(\frac{\partial P_1}{\partial \lambda}\bigg|_{\lambda=1,\lambda_T=1} \right)(\lambda - 1) + \left(\frac{\partial P_1}{\partial \lambda_T}\bigg|_{\lambda=1,\lambda_T=1} \right)(\lambda_T - 1), \tag{13}$$

$$\tilde{\sigma}_2 = \left(\frac{\partial P_2}{\partial \lambda}\bigg|_{\lambda=1,\lambda_T=1} \right)(\lambda - 1) + \left(\frac{\partial P_2}{\partial \lambda_T}\bigg|_{\lambda=1,\lambda_T=1} \right)(\lambda_T - 1). \tag{14}$$

After simplification, we obtain:

$$\tilde{\sigma}_1 = \left(\frac{4\mu}{3} + \frac{2}{D} \right)(\lambda - 1) + \left(-\frac{4\mu}{3} + \frac{4}{D} \right)(\lambda_T - 1), \tag{15}$$

$$\tilde{\sigma}_2 = \left(-\frac{2\mu}{3} + \frac{2}{D} \right)(\lambda - 1) + \left(\frac{2\mu}{3} + \frac{4}{D} \right)(\lambda_T - 1). \tag{16}$$

From the condition $P_2 = 0$, the transverse stretch can be expressed in closed form as:

$$\lambda_T = \frac{9 - 3\lambda + \mu D\lambda}{6 + \mu D}. \tag{17}$$

Note that the quantities $(\lambda - 1)$ and $(\lambda_T - 1)$ represent the engineering strains in the loading and transverse directions, respectively. Hence, the ground-state Poisson's ratio (ν_0) can be written in the following form:

$$\nu_0 = -\frac{\lambda_T - 1}{\lambda - 1} = \frac{3 - \mu D}{6 + \mu D} \;\rightarrow\; \mu D = 3\frac{1 - 2\nu_0}{1 + \nu_0}. \tag{18}$$

It is evident that the value of ν_0 depends on the product μD, and not on D alone. The ground-state Young's modulus (E_0) can also be computed by substituting the expression for λ_T (from Eq. 17) into the linearized stress formula:

$$\tilde{\sigma}_1 = E_0(\lambda - 1), \qquad E_0 = \frac{18\mu}{6 + \mu D}. \tag{19}$$

Knowing E_0 and ν_0, the ground-state shear (G_0) and bulk (K_0) moduli can be expressed as:

$$G_0 = \frac{E_0}{2(1 + \nu_0)} = \mu, \qquad K_0 = \frac{2}{D}. \tag{20}$$

It should be noted that the parameter α in the model has no influence on the values of the ground-state moduli. Using the expression obtained for ν_0, the original strain energy density function U can be reformulated such that the parameter D is eliminated and replaced with the parameter ν_0:

$$U = \mu \left(\frac{2}{\alpha^2}\left(\bar{\lambda}_1^\alpha + \bar{\lambda}_2^\alpha + \bar{\lambda}_3^\alpha - 3\right) + \frac{1 + \nu_0}{3(1 - 2\nu_0)}(J - 1)^2 \right). \tag{21}$$

Journal of Physics: Conference Series **3190** (2026) 012013 doi:10.1088/1742-6596/3190/1/012013

5 Analysis of uniaxial loading

It is important to note that even in the case of the first-order Ogden model, the transverse stretch λ_T cannot be expressed in a closed-form analytical relation based on Eq. 12. Consequently, in the compressible case, closed-form expressions for the stresses cannot be provided, even in the simplest uniaxial loading scenario, since determining the stress during loading requires knowledge of the corresponding λ_T value.

To understand the behavior of the material model under investigation, it is essential to analyze the character of transverse deformations that develop during uniaxial loading. From a practical standpoint, the model must follow physically meaningful trends. To establish a relationship between the axial stretch λ and the transverse stretch λ_T, the stress condition $\sigma_2 = \sigma_3 = 0$ must be imposed. Starting from the strain energy density function U and using equation (3), which specifies how the principal stresses σ_i are computed from the principal stretches λ_i, the stress components σ_2 and σ_3 can be written explicitly after substituting the expressions of the modified stretches and reformulating the material parameters in terms of the ground-state Poisson's ratio. Since $\mu \neq 0$, these expressions may be divided by μ for simplification. Imposing the conditions $\sigma_2 = \sigma_3 = 0$ then leads to the following nonlinear equation $R(\lambda, \lambda_T) = \sigma_2/\mu = \sigma_3/\mu$:

$$R(\lambda, \lambda_T) = \frac{2}{3}\left(\frac{1}{\alpha}\frac{\lambda^{-\alpha/3-1}}{\lambda_T^{2\alpha/3+2}}(\lambda_T^{\alpha} - \lambda^{\alpha}) + \frac{1+\nu_0}{1-2\nu_0}(\lambda\lambda_T^2 - 1)\right). \tag{22}$$

It is apparent that the expression $R(\lambda, \lambda_T)$ contains only two dimensionless material parameters: ν_0 and α. Therefore, the character of the transverse deformation is independent of the model parameter μ.

For given values of α and ν_0, the function $R(\lambda, \lambda_T)$ becomes an implicit equation in λ and λ_T. In general, this equation cannot be solved explicitly for $\lambda_T(\lambda)$, so a numerical approach must be applied. The arc-length method is a suitable choice here, since it is known that the point $\lambda = 1$ and $\lambda_T = 1$ is a valid solution of the equation. Thus, the arc-length based solution strategy can be initialized in both the tension and compression directions. For numerical calculations, we developed a custom arc-length algorithm in Wolfram Mathematica, and all simulations were carried out using this module with sufficiently small increments. In the present manuscript, we report only the solutions in the compression regime ($\lambda < 1$), as this is where the specific type of instability occurs that we aim to investigate. Here, instability refers to the condition in which, for a given axial stretch λ, multiple solutions exist for the transverse stretch λ_T. This definition of instability differs from the classical Drucker stability criterion.

The solutions obtained for λ_T are presented in Fig. 2 for four different values of α and various values of Poisson's ratio ν_0.

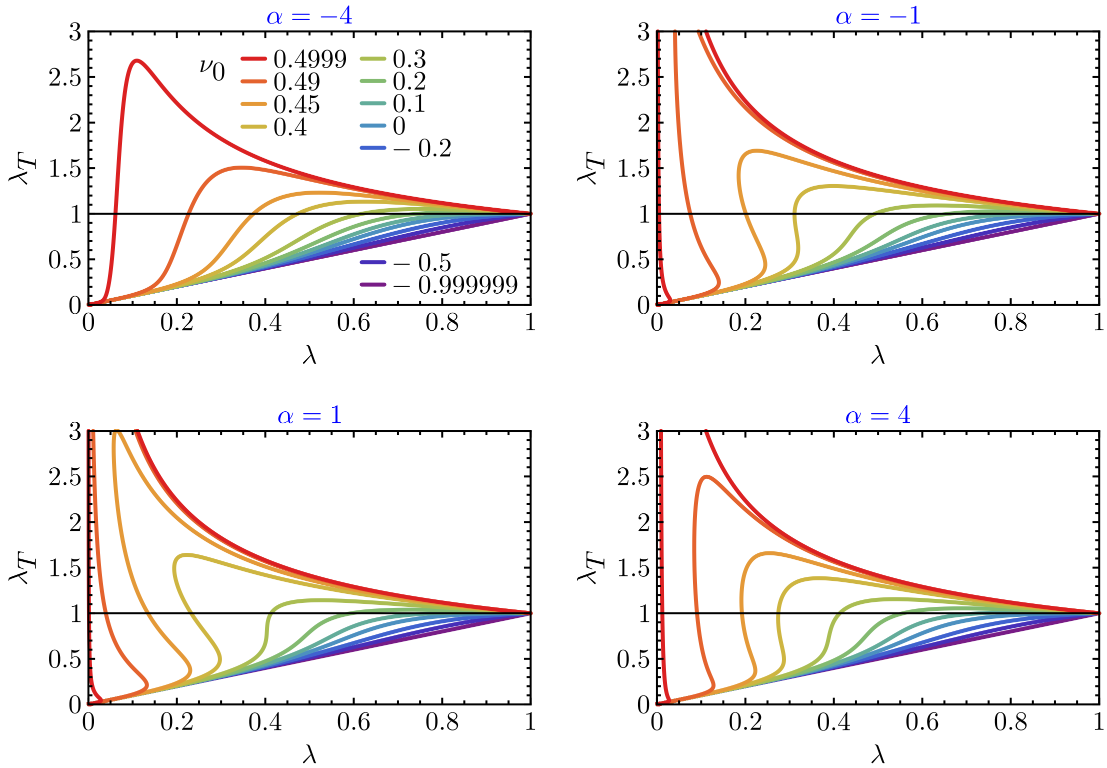

Figure 2: Variation of the transverse stretch under uniaxial loading for different values of α and ν_0. Each subfigure corresponds to a fixed α value, while the curves in different colors represent different ν_0 values.

It can be observed that for certain values of ν_0, the solution curve for λ_T reverses direction at a particular λ value, which implies physically unrealistic behavior of the model. From the numerical solutions, the critical value of ν_0 can be identified, beyond which this type of instability emerges. In Fig. 3, we present the domain in the $\lambda - \nu_0$ plane where three distinct solutions for λ_T exist for a given λ.

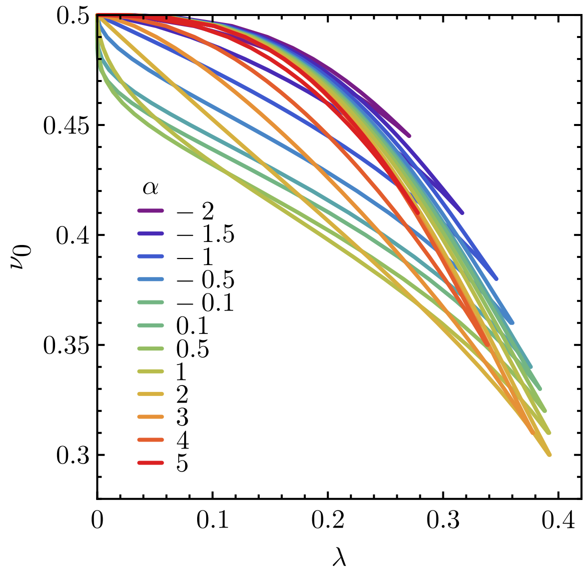

Figure 3: Instability domains under uniaxial loading shown in the $\lambda - \nu_0$ plane. The boundaries corresponding to different α values are indicated in different colors. The enclosed regions represent the instability domains.

From the perspective of practical application, it is essential to ensure that, for a given ν_0, the applied loading does not reach the critical value of λ where the instability domain begins. The results indicate that this instability region vanishes for $\alpha < -3$ and $6 < \alpha$. These numerical bounds represent conservative estimates; finer parameter discretization would yield more precise thresholds. The instability domain in the $\lambda - \nu_0$ plane reaches its largest extent near $\alpha = 0$. Thus, choosing $\alpha < -3$ or $6 < \alpha$ avoids the occurrence of multiple transverse stretch solutions for a given λ; however, the model may still exhibit physically unrealistic behavior at large deformations. It is also observed that if ν_0 is less than a critical value (approximately 0.3), the instability domain disappears regardless of the value of α.

Moreover, it is important to emphasize that for any value of ν_0, the transverse stretch approaches zero in the case of full uniaxial compression ($\lambda = 0$), meaning that the volume tends to zero, which is a physically unrealistic response.

6 Analysis of Equibiaxial and Planar loadings

For both the equibiaxial and planar loading cases, the condition $\sigma_3 = 0$ also results in a nonlinear equation that cannot be solved in closed form for the transverse stretch. Consequently, numerical methods are again required. For these loading scenarios, we also developed a custom arc-length-based numerical algorithm in Wolfram Mathematica, which was used to compute the corresponding transverse stretch values.

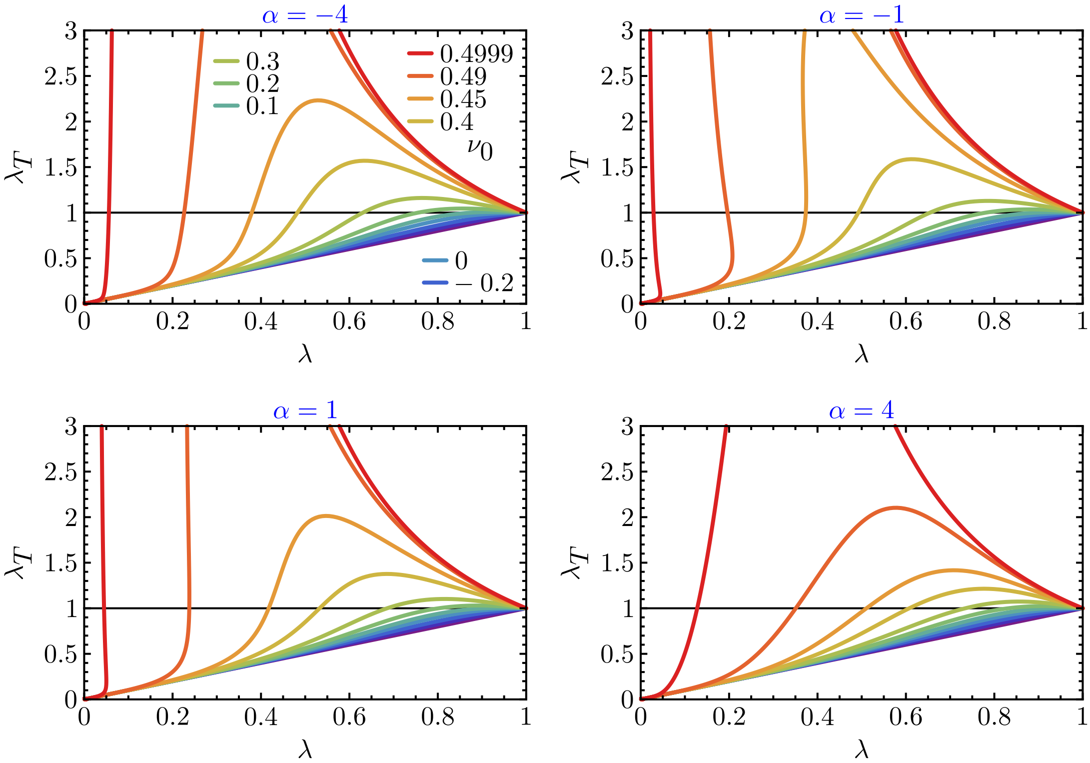

Figure 4: Variation of the transverse stretch under equibiaxial loading for different values of α and ν_0. Each subfigure corresponds to a fixed α value, while the curves in different colors represent different ν_0 values.

The transverse stretch solutions for equibiaxial loading are presented in Fig. 4 for the same values of the parameters α and ν_0 that were used for uniaxial loading in Fig. 2. From the analysis of the results, it can be concluded that even in this loading case, instability can occur for certain values of ν_0. It is also an important observation that, similarly to the uniaxial case, the transverse stretch value becomes zero under complete compression ($\lambda = 0$), which is again a physically unrealistic behavior. The instability domains—shown in Fig. 5 on the $\lambda - \nu_0$ plane—are, however, significantly smaller in extent for equibiaxial loading compared to the uniaxial case. Based on the discretization applied in α, we conservatively conclude that the instability region disappears when $\alpha < -1$ or $\alpha > 1.5$.

The transverse stretch values obtained under planar loading are presented in Fig. 6. From the analysis, it is evident that this loading condition also exhibits instability. The corresponding instability domains are illustrated in Fig. 7 on the $\lambda - \nu_0$ plane for various values of α. These domains are significantly smaller than those observed in the uniaxial loading case. Based on the discretization applied in the α and ν_0 parameters, we conservatively conclude that the instability domains appear only within the range $-3 < \alpha < 1.5$, similarly to the equibiaxial loading case.

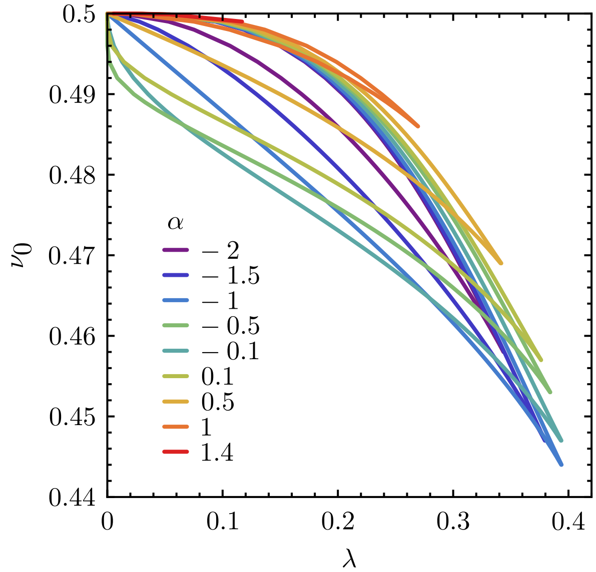

Figure 5: Instability domains under equibiaxial loading shown in the $\lambda - \nu_0$ plane. The boundaries corresponding to different α values are indicated in different colors. The enclosed regions represent the instability domains.

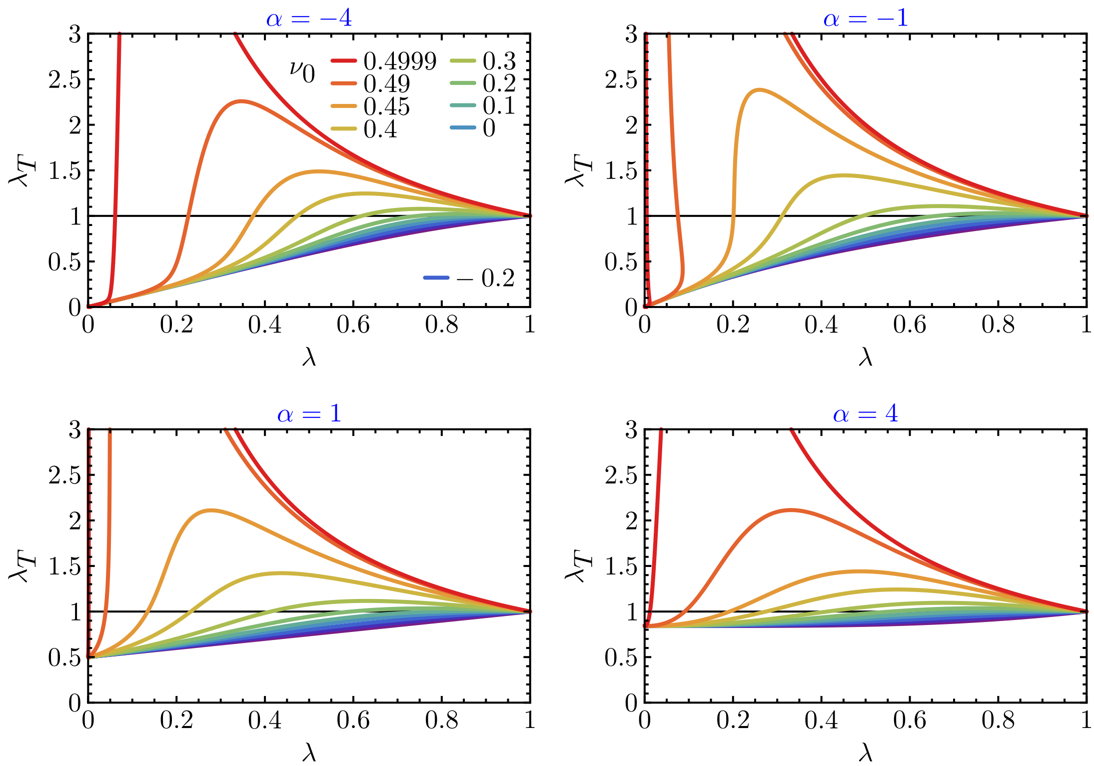

Figure 6: Variation of the transverse stretch under planar loading for different values of α and ν_0. Each subfigure corresponds to a fixed α value, while the curves in different colors represent different ν_0 values.

Journal of Physics: Conference Series **3190** (2026) 012013 doi:10.1088/1742-6596/3190/1/012013

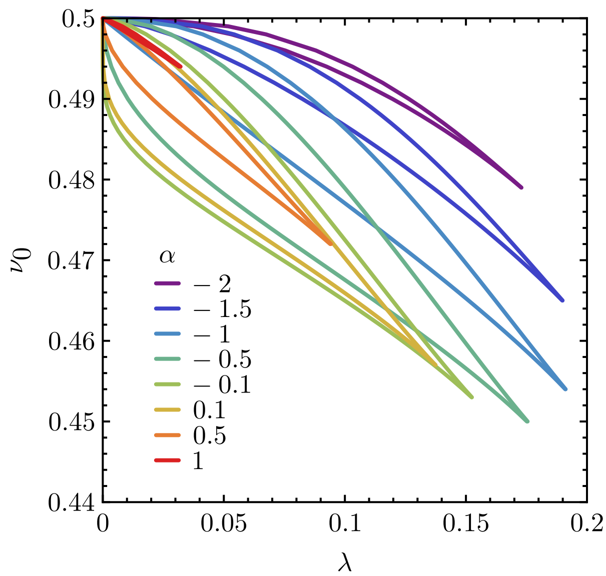

Figure 7: Instability domains under planar loading shown in the $\lambda - \nu_0$ plane. The boundaries corresponding to different α values are indicated in different colors. The enclosed regions represent the instability domains.

7 Conclusions

In the present study, we investigated the compressible, first-order Ogden hyperelastic model under three different homogeneous loading conditions: uniaxial, equibiaxial, and planar loading. We demonstrated that, under these loading states, the model may exhibit instability in terms of transverse deformation, which can result in the appearance of multiple possible solutions under compressive-type loading. Using numerical methods, we identified the critical combinations of the ground-state Poisson's ratio (ν_0) and the model parameter α at which this stability loss occurs. The analysis revealed that the extent of the instability domain strongly depends on both the ν_0 and α parameter values. Furthermore, it was also established that if the ground-state Poisson's ratio is below a certain critical threshold, the investigated instability vanishes entirely. In addition, we provided conservative estimates for the α parameter range in which transverse deformation-related instability can be avoided. The analytical framework and numerical methodology presented in this work can be extended to the stability analysis of other hyperelastic material models as well.

It should also be emphasized that the loss of stability is governed not only by the parameters α and ν_0, but by their combined interaction with the applied stretch λ, and the stability boundaries identified in this study arise from the joint dependence on all three quantities.

Although the present study has identified the stability domains for the three fundamental deformation modes examined, the results do not yet provide a fully comprehensive picture of the stability characteristics of the investigated hyperelastic model. Further analysis is required for general biaxial and triaxial loading scenarios, considering both stress-controlled and strain-controlled conditions. These investigations are intended to form the basis of future research efforts.

Journal of Physics: Conference Series **3190** (2026) 012013 doi:10.1088/1742-6596/3190/1/012013

8 Acknowledgments

This research was supported by the Hungarian National Research, Development and Innovation Office (FK 142457). This research was supported by the János Bolyai Research Scholarship of the Hungarian Academy of Sciences.

References

[1] B. Fodor and A. Kossa. Stability study of the compressible Mooney-Rivlin hyperelastic model. *The Journal of Strain Analysis for Engineering Design*, 59(4):258–268, 2024. doi: 10.1177/03093247241233712.

[2] H. He, Q. Zhang, Y. Zhang, J. Chen, L. Zhang, and F. Li. A comparative study of 85 hyperelastic constitutive models for both unfilled rubber and highly filled rubber nanocomposite material. *Nano Materials Science*, 4(2):64–82, 2022. doi: 10.1016/j.nanoms.2021.07.003.

[3] G. A. Holzapfel. In *Nonlinear Solid Mechanics*. Wiley, 2010.

[4] A. Kossa. Closed-form analytical solutions for stability bounds of the incompressible Mooney-Rivlin hyperelastic model under standard homogeneous loadings. *International Journal of Applied Mechanics*, 17(3):1–27, 2025. doi: 10.1142/S1758825125500152.

[5] A. Kossa, M. T. Valentine, and R. M. McMeeking. Analysis of the compressible, isotropic, neo-Hookean hyperelastic model. *Meccanica*, 58(1):217–232, 2023. doi: 10.1007/s11012-022-01633-2.

[6] R.W. Ogden. In *Non-linear Elastic Deformations*. Dover, 1997.

[7] A. Ricker and P. Wriggers. Systematic fitting and comparison of hyperelastic continuum models for elastomers. *Archives of Computational Methods in Engineering*, 30(3):2257–2288, 2023. doi: 10.1007/s11831-022-09865-x.